

## Proton halos in the $1s0d$ shell

B.A. Brown, P.G. Hansen

Department of Physics and Astronomy and National Superconducting Cyclotron Laboratory, Michigan State University,  
East Lansing, MI 48824, USA

Received 10 April 1996; revised manuscript received 15 May 1996

Editor: C. Mahaux

---

### Abstract

The shell-model properties of proton halo states in proton-rich  $1s0d$  shell nuclei are investigated. The most interesting cases appear to be those in  $^{26,27}\text{P}$  and  $^{27}\text{S}$ . The parallel-momentum distributions of core fragments from proton stripping reactions may provide experimental insight into the structure of the halo states and the role played by the reaction mechanism. The “generalized Coulomb shift”, defined as the difference between the neutron and proton separation energies for an analogue pair, is shown to vary smoothly as a function of proton-separation energy and provides a good tool for mass extrapolations. The relation between the total interaction cross section and the matter radius is discussed.

PACS: 21.10.Dr; 21.10.Ft; 21.10.Gv; 21.60.Cs; 25.60.Gc; 27.30.+t

Keywords: Proton halo; Neutron halo; Breakup momentum distribution; Shell model; Coulomb shift

---

Nuclei near the proton and neutron drip lines often have matter distributions which extend to large radii due to the loose binding of the last one or two nucleons. The extended distributions are referred to as “halos”. [1,2] The halo has been observed experimentally from an increase of the total reaction cross section, which is related to the total matter density, and from the momentum distribution in break-up reactions, which is related to the density of the valence orbital. One of the simplest ground-state examples is  $^{11}\text{Be}$  where the last neutron is predominantly in a  $1s_{1/2}$  state [3] and is bound only by 0.50 MeV. The density distribution of the valence neutron is extended with an rms radius [2,4,5] of about 6.0 fm, and the parallel-momentum distribution in the reaction ( $^{11}\text{Be}, ^{10}\text{Be}$ ) is correspondingly narrow, [6]  $42 \pm 2$  MeV/c for a light target, due of the loose binding, and because there is no centrifugal or Coulomb barrier. A similar case [7,8] is

$^{19}\text{C}$ . Other examples [1,2,5] on the neutron-rich side are the loosely bound di-neutron systems such as  $^{11}\text{Li}$  and  $^{14}\text{Be}$ .

The analogues of the cases mentioned above on the proton-rich side are all unbound. Perhaps the simplest example of a bound-state proton halo is that of the  $1/2^+$  first excited state of  $^{17}\text{F}$  which is bound by 0.10 MeV. This state is described in zeroth order by a  $1s_{1/2}$  configuration outside of an  $^{16}\text{O}$  closed shell, and has a calculated [9] rms valence radius of 5.5 fm. However, since this is an excited state its reaction cross section and momentum distribution cannot be studied, and its proton halo nature is inferred from the large Thomas-Ehrman Coulomb shift relative to the  $5/2^+ T = 1/2 (0d_{5/2})$  ground state [10,11] and from the large  $1/2^+$  to  $5/2^+$   $\text{B(E2)}$  value [9]. In general, for a fixed angular momentum and fixed separation energy, the size of the proton halo states are not as large

Table 1

One-neutron separation energies for mirror pairs based on the compilation of Audi and Wapstra [18]. Numbers in square brackets are based upon the Audi and Wapstra mass systematics.

Z	N	Nucleus	$S_p$	Mirror nucleus	$S_n$	$\Delta_{np} = S_n - S_p$
15	14	$^{29}\text{P}$	2.748	$^{29}\text{Si}$	8.473	5.725
	13	$^{28}\text{P}$	2.066(4)	$^{28}\text{Al}$	7.725	5.660(4)
	12	$^{27}\text{P}$	0.897(35)	$^{27}\text{Mg}$	6.443	5.546(35)
	11	$^{26}\text{P}$	[0.14(20)]	$^{26}\text{Ne}$	5.616(14)	[5.47(20)]
	10	$^{25}\text{P}$	[-0.83(20)]	$^{25}\text{F}$	4.182(46)	[5.01(20)]
	9	$^{24}\text{P}$	[-0.8(5)]	$^{24}\text{O}$	3.86(10)	[4.8(5)]
16	15	$^{31}\text{S}$	6.133	$^{31}\text{P}$	12.311	6.178
	14	$^{30}\text{S}$	4.400(3)	$^{30}\text{Si}$	10.609	6.209(3)
	13	$^{29}\text{S}$	3.287(50)	$^{29}\text{Al}$	9.436	6.149(50)
	12	$^{28}\text{S}$	[2.46(16)]	$^{28}\text{Mg}$	8.504(2)	[6.04(16)]
	11	$^{27}\text{S}$	[0.75(28)]	$^{27}\text{Na}$	6.750(41)	[5.99(29)]
	10	$^{26}\text{S}$	[0.19(36)]	$^{26}\text{Na}$	5.582(71)	[5.39(36)]

as the neutron halo states because of the Coulomb barrier.

The only case on the proton-rich side whose break-up distribution of parallel momentum<sup>1</sup> has been studied is that of  $^8\text{B}$ . The valence proton in this case is bound by 0.137 MeV and the calculated [12] valence  $0p$  proton rms radius is 4.4 fm. Its measured momentum distribution [13,14] is, however, almost a factor of two narrower than that predicted from the Fourier transform of the spatial wave function of the valence nucleon, and this is presumably [12,15] related to the fact that the proton stripping reaction only samples the valence density beyond a minimum impact parameter  $b_{\min}$ . This can be defined as the sum of the (experimentally determined) energy-dependent interaction radii of the core fragment and the target. For  $^8\text{B}$  incident at 1.47 GeV/u on a carbon target one has a  $b_{\min}$  of 4.8 fm. An estimate based on an eikonal picture can account both for the momentum content of the halo wave function and for the absolute cross section, which can be linked to that for free nucleons of the same velocity. The effects of the localization of the reaction to the external part of the wave function

are strongly dependent on the separation energy of the halo nucleon and its angular momentum. In the case of a neutron in an  $s$  state with parameters corresponding to those of  $^{11}\text{Be}$ , the momentum width is rather close to that of the wave function as a whole, which is probably why the localization effect was not considered in early discussions of the parallel-momentum distributions.

The main thing missing from the cases discussed above is a good example of a proton-rich ground state whose structure is that of a valence proton  $s_{1/2}$  orbital coupled to the ground state of the core. The natural place to look for such a configuration is in the middle of the  $1s0d$  shell at the nuclei with  $Z = 15$  and  $Z = 16$ , where in the simplest shell-model picture the  $1s_{1/2}$  orbital becomes filled. An example is  $^{29}\text{P}$  which is well known [16] to have a zeroth-order structure of a  $1s_{1/2}$  proton outside a  $^{28}\text{Si}$  closed shell, but its structure is not as simple as that of  $^{17}\text{F}$ , and the full- $1s0d$  shell configuration mixing is needed [16,17] in order to explain the magnetic properties of  $^{29}\text{P}$  and its mirror  $^{29}\text{Si}$ . It is interesting to examine the properties of the more neutron-deficient isotopes of phosphorus ( $Z = 15$ ).

The one-proton separation energies,  $S_p$ , for the  $Z = 15, 16$  isotopes [18] as a function of neutron number  $N$  are given in Table 1. These are compared with the one-neutron separation energies,  $S_n$ , for  $N = 15, 16$  as a function of proton number. The difference  $\Delta_{np} = S_n - S_p$ , is also given. It is clear that  $^{26}\text{P}$  is potentially

<sup>1</sup> In the present paper we restrict the discussion of momentum distributions to the parallel momentum measured in reactions such as  $(^{26}\text{P}, ^{25}\text{Si})$  etc. on light targets because this parameter seems particularly simple to interpret. It should be clear that valuable additional characterization of halo states can be obtained from the transverse momentum components and from Coulomb excitation of the halo.

the most interesting loosely bound case, as has been pointed out recently on the basis of relativistic mean-field calculations [19], and it is known [20] to be particle-stable. The value of  $S_p$  has been derived [18] from systematic extrapolations, and the large error bars assigned to it and to some of the other cases by Audi and Wapstra [18] are only of symbolic significance.

The quantity  $\Delta_{np}$  is the generalized Coulomb shift for mirror pairs. It is not surprising that it is almost constant: owing to nuclear charge symmetry and the long-range Coulomb force, the shift is a pure Coulomb effect and is very insensitive to the details of the nuclear wave functions. It can be modeled by calculating the proton and neutron single-particle energies in a Woods-Saxon potential which has a Coulomb potential plus a common central potential for protons and neutrons. By varying the depth and/or radius of the central potential one can calculate the relationship between  $S_p$  and  $\Delta_{np}$ . The results for a typical Woods-Saxon potential are shown in Fig. 1. The solid line is the result obtained by varying the nuclear well depth from  $V_o = 42$  MeV to  $V_o = 54$  MeV for a fixed radius ( $R = 3.89$  fm) and diffuseness ( $a = 0.65$  fm), and the dashed line is the result obtained by varying the radius from  $r_o = 1.17$  fm to  $r_o = 1.36$  fm ( $R = r_o A^{1/3}$ ) for a fixed well depth ( $V_o = 48$  MeV) and diffuseness ( $a = 0.65$  fm). These parameters are all within the range expected. The main point is that the calculated dependence of  $\Delta_{np}$  upon  $S_p$  is very smooth even very close to the proton threshold (when  $S_p$  goes to zero). This is because of the relatively large Coulomb barrier. The experimental values show a similar smooth behavior, which suggests that the  $S_p$  value for  $^{26}\text{P}$  cannot be far from the Audi-Wapstra extrapolation of 0.14 MeV. (The overall shift between the experimental and theoretical values is related to the Nolen-Schiffer anomaly and as well as the various exchange-interaction and relativistic corrections which are left out of the calculation [10].)

The slope for the  $1s_{1/2}$  state seen in Fig. 1 is related to the Thomas-Ehrman shift for the  $1s_{1/2}$  halo state. It is interesting to compare these results for the  $1s_{1/2}$  configuration to those for the isotopes with  $Z = 13, 14$  which should be dominated by a  $0d_{5/2}$  valence configuration, see Fig. 1. In this case the experimental values for  $\Delta_{np}$  are essentially flat as a function of  $S_p$ , and this is reproduced by the calculation. The calculated curve for  $0d_{5/2}$  shows a smaller slope relative

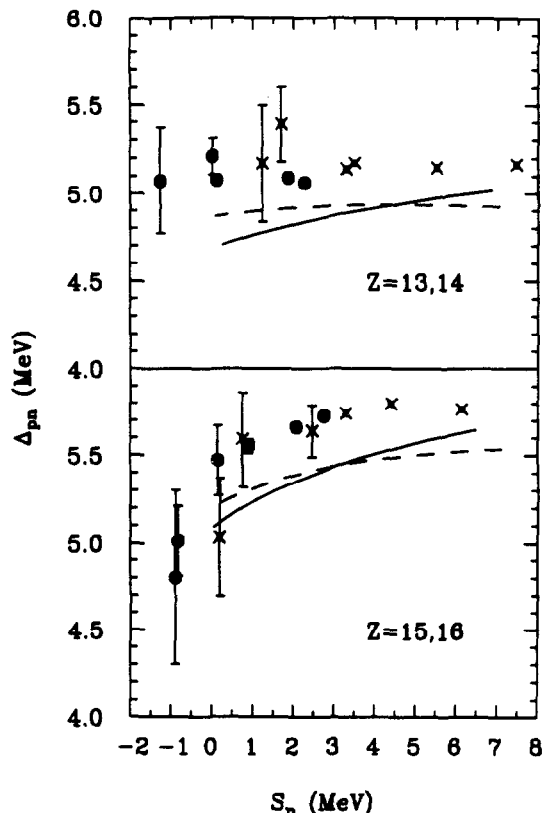


Fig. 1.  $\Delta_{np}$  vs  $S_p$ . The experimental results [18] for  $Z = 13$  and  $Z = 15$  are given by the filled circles. The experimental results for  $Z = 14$  and  $Z = 16$  multiplied by  $(13/14)$  and  $(15/16)$ , respectively, are given by crosses. The solid and dashed lines for  $Z = 13, 14$  are the  $0d_{5/2}$  calculations discussed in the text. The solid and dashed lines for  $Z = 15, 16$  are the  $1s_{1/2}$  calculations discussed in the text.

to  $0s_{1/2}$  due to the centrifugal barrier for  $\ell=2$ .

The case of  $^{26}\text{P}$  is more complicated than the usual one-nucleon halos because it has an odd number of both neutrons and protons. Most likely its spin is 3, the same as that of its mirror nucleus  $^{26}\text{Na}$  measured by atomic spectroscopy [21]. Shell-model calculations with the USD [22] and SDPTA [23]  $1s0d$  shell-model interactions suggest the presence of a low-lying quartet arising from the coupling of the odd  $1s_{1/2}$  neutron to the  $5/2^+$  ground state and  $3/2^+$  low-lying (0.090 MeV) excited state in  $^{25}\text{Na}$ . The order of the levels in the quartet is very sensitive to the interaction, with the SDPTA interaction obtaining the correct assignment of  $3^+$  for the ground state. The beta decay of  $^{26}\text{Ne}$  leads [24,25,26] to other low-lying states in

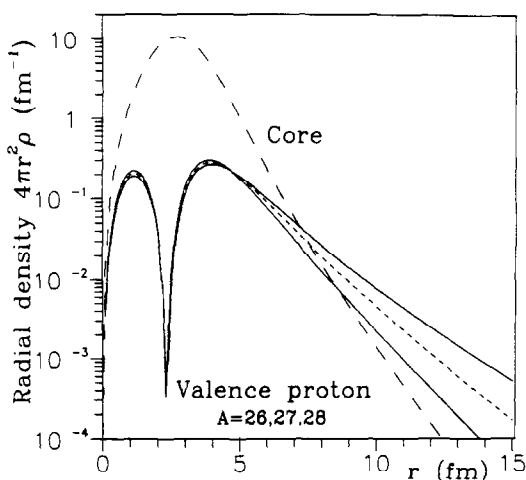


Fig. 2. The radial density probability distribution of the core and of the valence proton, the latter calculated in a single particle Woods-Saxon model for  $^{26,27,28}\text{P}$  with proton separation energies assumed to be 0.14, 0.90 and 2.07 MeV, respectively. The valence proton distribution is normalized to unity. [These calculations use  $r_0 = 1.25$  fm,  $a = 0.7$  fm and an (adjustable) well-depth near 41 MeV.]

$^{26}\text{Na}$  including [27,25] a  $1^+$  at 0.082 MeV. It is therefore not inconceivable that the Coulomb effects would be strong enough to shift the order of the mirror states in  $^{26}\text{P}$ .

Still, the most likely spin for the ground state of the mirror nucleus  $^{26}\text{P}$  is  $3^+$ . The calculated [28] half-life of 38 ms based upon a  $3^+$  assignment is consistent with the observed half-life [20] of  $20^{+35}_{-15}$  ms. In the full  $0d1s$  shell-model calculation its main parentage is to the  $5/2^+$  ground state of  $^{25}\text{Si}$  with a  $1s_{1/2}$  spectroscopic factor of  $C^2S = 0.66$  (to be compared with  $C^2S = 1.0$  in the zeroth-order shell model). The  $0d_{5/2}$  spectroscopic factor is very small (0.002). The total proton occupation of the  $1s_{1/2}$  orbital is 1.05 and the remaining 0.39 of the  $1s_{1/2}$  spectroscopic strength goes to highly excited  $5/2^+$  and  $7/2^+$  states in  $^{25}\text{Si}$ . The halo structure of  $^{26}\text{P}$  should thus be calculated as if it were 0.66 of  $1s_{1/2}$  proton bound by about 0.14 MeV to the  $^{25}\text{Si}$  ground state. In a typical Woods-Saxon geometry (the same one used in the discussion above), the rms radius of the  $1s_{1/2}$  state is 4.71 fm. This can be compared to the total proton and neutron rms radius of the  $^{25}\text{Si}$  core of 3.35 fm and 2.86 fm, respectively, see Fig. 2.

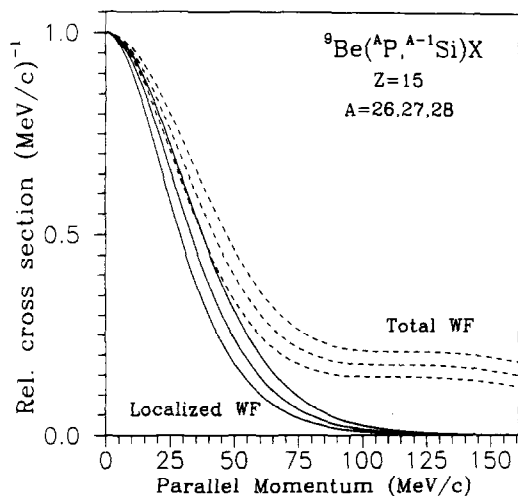


Fig. 3. The parallel-momentum distributions calculated for the  $^{26,27,28}\text{P}$  proton halos with parameters as in Table 1 and Fig. 2. The curves for mass 26 are those most to the left. The dashed curves represent the result for the total wave function. The full-drawn curves take into account that the interaction with the target (taken to be  $^9\text{Be}$ ) localizes the observation to distances beyond the minimum impact parameter. Note that in the latter case the complete disappearance of the plateau around 100–150 MeV/c representing the inner lobe of the spatial wave functions (Fig. 2).

The behavior of the single-particle proton<sup>2</sup> wave functions at large distances is dominated by the Coulomb barrier and the sensitivity to the proton separation energy is not large. This can be seen from the comparison of the radial densities for  $^{26,27,28}\text{P}$  shown in Fig. 2, and which correspond to rms radii of 4.71, 4.37 and 4.11 fm, respectively. For comparison a corresponding 1s state neutron with an  $S_n$  of 0.14 MeV would have a radius of about 10.8 fm.

Not surprisingly, the calculated parallel-momentum distributions shown in Fig. 3 mirror closely the behavior of the spatial wave functions. The approximation [15] used here for calculating the localization effect replaces the wave function in the tube swept by the target nucleus by its values along the axis defined by the impact parameter, the minimum of which is

<sup>2</sup> A potential-well model is expected to work well for the phenomena discussed in the present paper. Both the Coulomb energy shifts (Fig. 1) and the parallel-momentum distributions in stripping (Fig. 3) reflect essentially the asymptotic behavior of the s-wave proton, and the complex-structure admixtures, which reduces the spectroscopic factor to 0.66, will mainly effect the normalization.

Table 2

Two-nucleon separation energies for mirror pairs based on the compilation of Audi and Wapstra [18]. Numbers in square brackets are based upon the Audi and Wapstra mass systematics.

Z	N	Nucleus	$S_{2p}$	Mirror nucleus	$S_{2n}$	$\Delta_{2n2p} = S_{2n} - S_{2p}$
14	13	$^{27}\text{Si}$	13.770	$^{27}\text{Al}$	24.424	10.654
	$^{26}\text{Si}$	7.789(3)	$^{26}\text{Mg}$	18.424	10.634(3)	
	11	$^{25}\text{Si}$	5.280(10)	$^{25}\text{Na}$	15.971	10.691(10)
	10	$^{24}\text{Si}$	3.426(20)	$^{24}\text{Ne}$	14.066(10)	10.639(22)
	9	$^{23}\text{Si}$	[11.72(20)]	$^{23}\text{F}$	12.766(80)	[11.05(21)]
	8	$^{22}\text{Si}$	[-0.02(20)]	$^{22}\text{O}$	10.655(57)	[10.67(21)]
16	15	$^{31}\text{S}$	11.728	$^{31}\text{P}$	23.632	11.904
	14	$^{30}\text{S}$	7.148(3)	$^{30}\text{Si}$	19.083	11.935(3)
	13	$^{29}\text{S}$	5.352(50)	$^{29}\text{Al}$	17.161	11.809(50)
	12	$^{28}\text{S}$	[3.36(16)]	$^{28}\text{Mg}$	14.947(2)	[11.59(16)]
	11	$^{27}\text{S}$	[0.90(20)]	$^{27}\text{Na}$	12.366(38)	[11.47(21)]
	10	$^{26}\text{S}$	[-0.64(30)]	$^{26}\text{Na}$	9.765(56)	[10.40(30)]

6.2 fm for the case of a  $^9\text{Be}$  target. Due to the strong effect of the Coulomb barrier, which makes the external wave function fall off more rapidly, this approximation is less accurate than previous estimates [15] for lighter systems. It should give reasonable values for the momentum distributions but will underestimate the cross sections. For an assumed beam energy of 60 MeV/u and for phosphorus isotopes with masses 26, 27 and 28, the calculated localized widths are 58 (74), 66 (84) and 75 (94) MeV/c, respectively, for the full width at half maximum. The values in parentheses are those calculated for the total wave function. The corresponding calculated cross sections (assuming  $C^2 S = 1$ ) are 51, 35 and 22 mb, respectively, very similar to those of single-nucleon knock-out reactions on systems with normal binding. (The cross section obtained for the total wave function is 720 mb for all three cases.)

It is feasible and should be very interesting to study the parallel momentum distributions experimentally. The best illustration [12,15] of the localization effect so far, that of the  $^8\text{B}$   $0p$  state, has a single lobe in the wave function and the effect shows up as a narrowing of the observed distribution. In contrast to this, the absence in the phosphorus isotopes of the large momentum components corresponding to the inner lobe of the  $1s$  state will provide another experimental signature for the contribution from the reaction mechanism.

It is also interesting to investigate the proton-halo aspects of the  $Z = 16$  isotopes. The one-proton sepa-

ration energies are summarized in Table 1 and Fig. 1. It would appear from the Audi-Wapstra mass systematics that  $^{26}\text{S}$  could be a loosely bound system, and this would be particularly interesting since the corresponding daughter nucleus  $^{25}\text{P}$  is itself unbound. However, from the  $\Delta_{np}$  systematics it is clear that  $\Delta_{np}$  should be close to 6.0 MeV which when combined with  $S_n$  for  $^{26}\text{Na}$  would make  $^{26}\text{S}$  unbound by 0.42 MeV. In addition,  $^{26}\text{S}$  is unbound to two-proton emission (see Table 2).  $^{27}\text{S}$  has a separation energy of 0.75 MeV. The properties of the  $1s_{1/2}$  halo in  $^{27}\text{S}$  should be very similar to that of  $^{27}\text{P}$  shown in Figs. 2 and 3, since the one-proton separation energy is about the same in both cases. As pointed out in Ref. [19],  $^{27}\text{S}$  also has the property of a relatively loosely bound di-proton system. The two-proton separation energies for  $Z = 16$  are given in Table 2. It would be very interesting to try to apply the three-body techniques which have been used for  $^{11}\text{Li}$  to the case of  $^{27}\text{S}$ .

Finally, we note the case of  $^{22}\text{Si}$  which is known [29] to be particle-stable but which has (see Table 2) a small two-proton separation energy. We have used the SGII Skyrme interaction [30] to carry out Hartree-Fock calculations for the proton and neutron densities of light nuclei [5,31]. (HF calculations for the  $1s_{1/2}$  proton halos discussed above are indistinguishable from the Woods-Saxon calculations discussed, as long as the proton separation energy is fixed at the experimental value.) The results of such calculations for the rms matter radii of  $^{22}\text{Si}$  and  $^{22}\text{O}$

are 3.08 fm and 3.00 fm, respectively. Thus even though the  $0d_{5/2}$  is loosely bound in  $^{22}\text{Si}$ , the rms matter radius is only 2.5 percent larger; again this is due to the  $\ell=2$  centrifugal barrier and the Coulomb barrier. Although this case has not yet been studied, the total interaction cross sections for a similar pair of nuclei,  $^{20}\text{Mg}$  and  $^{20}\text{O}$  has recently been reported [32]. The Glauber model has been used to interpret the observed 7 percent increase in the  $^{20}\text{Mg}$  cross section relative to  $^{20}\text{O}$  as being related to a 6–8 percent increase in the rms matter radius. However, as above, the calculated rms matter radii for  $^{20}\text{Mg}$  and  $^{20}\text{O}$  are more nearly equal; 2.85 fm and 2.80 fm respectively. It has also been noted [33] that the  $A = 20$  Coulomb shifts are not consistent with a halo and that perhaps an exotic “tetra-proton” structure is needed to explain the radius change. However, the relationship between the matter radii and the total interaction cross sections may not be a simple as that given by the standard Glauber model interpretation, especially for nuclei near the drip lines. We note that  $^{20}\text{Mg}$  with a proton separation energy of 2.65 MeV has only one bound excited state (a  $2^+$  state at about 1.7 MeV) as compared to  $^{20}\text{O}$  with a neutron separation energy of 7.61 MeV which has many bound states. Thus the part of the total interaction cross section leading to states between 3 and 8 MeV in excitation energy will be part of the measured reaction cross section for  $^{20}\text{Mg}$ , but will not contribute for  $^{20}\text{O}$ , since the nucleus decays back to the ground state and is detected as  $^{20}\text{O}$ . The size of this effect should be calculated or measured.

This research was partly supported by the National Science Foundation grants PHY-94-03666 and PHY-95-28844.

## References

- [1] A.C. Mueller and B.M. Sherrill, *Annu. Rev. Nucl. Part. Sci.* 43 (1993) 529.
- [2] P.G. Hansen, A.S. Jensen and B. Jonson, *Annu. Rev. Nucl. Part. Sci.* 45 (1995) 591.
- [3] H. Sagawa, B.A. Brown and H. Esbensen, *Phys. Lett. B* 309 (1993) 1;
- T. Otsuka, N. Fukunishi and H. Sagawa, *Phys. Rev. Lett.* 79 (1993) 1385;
- H. Esbensen, B.A. Brown and H. Sagawa, *Phys. Rev. C* 51 (1995) 1274.
- [4] D.J. Millener, J.W. Olness, E.K. Warburton and S.S. Hanna, *Phys. Rev. C* 28 (1983) 497.
- [5] G.F. Bertsch, B.A. Brown and H. Sagawa, *Phys. Rev. C* 39 (1989) 1154.
- [6] J.H. Kelley et al., *Phys. Rev. Lett.* 74 (1995) 30.
- [7] D. Bazin et al., *Phys. Rev. Lett.* 74 (1995) 3569.
- [8] F.M. Marques et al., IPC CAEN preprint LPCC 96-05.
- [9] B.A. Brown, A. Arima and J.B. McGrory, *Nucl. Phys. A* 277 (1977) 77.
- [10] J. Nolen and J.P. Schiffer, *Annu. Rev. Nucl. Sci.* 19 (1969) 471.
- [11] R. Sherr and G. Bertsch, *Phys. Rev. C* 32 (1985) 1809.
- [12] B.A. Brown, A. Csoto and R. Sherr, *Nucl. Phys. A* 597 (1996) 66.
- [13] W. Schwab et al., *Z. Phys. A* 350 (1995) 283.
- [14] J.H. Kelley et al., *Bull. Am. Phys. Soc.* 40 (1995) 978.
- [15] P.G. Hansen, Proceedings of the International Conference on Exotic Nuclei and Atomic Masses Conference, Arles 1995, eds. M. de Saint Simon and O. Sorlin (Editions Frontieres), in press, and to be published.
- [16] B.A. Brown, *Nucl. Phys. A* 522 (1991) 221c.
- [17] B.A. Brown, R. Radhi and B.H. Wildenthal, *Phys. Lett. B* 133 (1983) 5.
- [18] G. Audi and A.H. Wapstra, *Nucl. Phys. A* 595 (1995) 409.
- [19] Z. Ren, B. Chen, Z. Ma and G. Xu, *Phys. Rev. C* 53 (1996) R572.
- [20] M.D. Cable et al., *Phys. Lett. B* 123 (1983) 25.
- [21] G. Huber et al., *Phys. Rev. C* 18 (1978) 2342.
- [22] B.A. Brown and B.H. Wildenthal, *Annu. Rev. Nucl. Sci.* 38 (1988) 29.
- [23] B.A. Brown, W.A. Richter, R.E. Julies and B.H. Wildenthal, *Ann. Phys.* 182 (1988) 191.
- [24] J.P. Dufour et al., *Z. Phys. A* 324 (1986) 487.
- [25] J.P. Dufour, private communication.
- [26] B.H. Wildenthal, M.S. Curtin and B.A. Brown, *Phys. Rev. C* 28 (1983) 1343.
- [27] P.M. Endt, *Nucl. Phys. A* 521 (1990) 1.
- [28] B.A. Brown, *Phys. Rev. Lett.* 65 (1990) 2753.
- [29] M.G. Saint-Laurent et al., *Phys. Rev. Lett.* 59 (1987) 33.
- [30] N. van Gaij and H. Sagawa, *Nucl. Phys. A* 371 (1981) 1; N. van Gaij and H. Sagawa, *Phys. Lett. B* 106 (1981) 379.
- [31] B.A. Brown and W.A. Richter, unpublished.
- [32] L. Chulkov et al., GSI preprint 95-75 (1995).
- [33] L. Chulkov, E. Roeckl and G. Kraus, *Z. Phys. A* 353 (1996) 351.